Matthias Heger, Tina Scharge[‡], and Martin A. Suhm[*]

Institute of Physical Chemistry, Georg-August-Universität,

Tammannstraße 6, 37077 Göttingen, Germany. E-mail: msuhm@gwdg.de

[‡] *Current address: Gesellschaft für Anlagen- und Reaktorsicherheit (GRS) mbH,*

Schwertnergasse 1, 50667 Köln

From hydrogen bond donor to acceptor: The effect of ethanol fluorination on the first solvating water molecule

Supplementary information

Complete Basis Set Limit Extrapolations

Quantum-chemical calculations typically employ one-electron basis sets of Gaussian functions to ease their computational demand. However, the mathematical incompleteness of finite basis sets introduces errors to the calculations, most notably the basis set superposition error (BSSE). As a method of estimating basis set incompleteness penalties, we employed extrapolations to the complete basis set (CBS) limit including higher-order electron correlation. The less problematic Hartree-Fock energies were treated by a scheme by Jensen[1] in the $\gamma = 9$ refinement by Karton and Martin[2] so that the energy at the CBS limit (E_{CBS}) is given by

$$E_{\mathrm{CBS}} = E_5 + \frac{E_5 - E_4}{\frac{5}{6}\exp\left(9\left(\sqrt{5}-\sqrt{4}\right)\right) - 1} = E_5 + 0.167\,(E_5 - E_4)$$

with E_4 and E_5 denoting the Hartree-Fock energies calculated in the aug-cc-pVQZ and aug-cc-pV5Z basis sets, respectively. The correlation contributions were extrapolated using the elaborate "Ave-CCSD(T)/D + Ave-ΔMP2((Q-T)-D)" scheme by Mackie and DiLabio[3] which was crafted to model non-covalent intermolecular interactions. Specifically, the correlation contribution obtained from a MP2/aug-cc-pVDZ calculation is subtracted from a two-point extrapolation based on the aug-cc-pVTZ and aug-cc-pVQZ basis sets, yielding a "MP2((Q-T)-D)" value to which the correlation energy of a CCSD(T)/aug-cc-pVDZ ("CCSD(T)/D") calculation is added. "Ave" indicates that all energies are averaged between CP- and non-CP-corrected values (i.e., only half of the CP energy correction is applied to each individual value), since such averaging provides much faster convergence of the energies to the CBS limit.[3] An alternative would be

the use of explicitly correlated wavefunctions.[4,5] The structures employed in the extrapolations for the fluoroethanols were optimized at the MP2/aug-cc-pVTZ level. The absolute dissociation energies of the $\mathbf{e}^{\mathrm{M}}\mathbf{w}$ and $\mathbf{we}^{\mathrm{M}}$ complexes show considerable deviations between the CBS extrapolations and the MP2/6-311++G(d,p) approach employed throughout our study (see the table below); however, the energy gap between these structures appears to be quite adequately modeled by the MP2/6-311++G(d,p) calculations, due to a lucky amount of error compensation in the method and basis set. In comparison, the B3LYP/6-311++G(d,p) dissociation energies are already close to the best extrapolated values, despite the neglect of dispersion interactions. If the latter are accounted for, the dissociation energies are drastically overestimated. None of the employed approaches should thus be trusted on an absolute binding energy scale.

Table S1: Absolute electronic energies E_{abs} (in Hartree) and dissociation energies D_{e} (in kJ/mol, without zero-point correction) for mixed $\mathbf{w}/\mathbf{e}^{\mathrm{M}}$ complexes and fully optimized monomers from MP2, B3LYP and B3LYP-D3 calculations using the 6-311++G(d,p) ("6311") and aug-cc-pVTZ ("aVTZ") basis sets; also given are the results from CBS limit extrapolations (see text). All structures were optimized at the respective level of theory, except for the CBS calculations which used the MP2/aVTZ structures.

	MP2/6311		MP2/aVTZ		CBS limit	
	E_{abs}	D_e	E_{abs}	D_e	E_{abs}	D_e
$\mathbf{w}$	−76.274921		−76.328992		−76.376555	
$\mathbf{e}^{\mathrm{M}}$	−253.722336		−253.894385		−254.057658	
$\mathbf{e}^{\mathrm{M}}\mathbf{w}$	−330.010215	34.0	−330.235833	32.7	−330.446119	31.3
$\mathbf{we}^{\mathrm{M}}$	−330.008666	30.0	−330.234363	28.8	−330.444509	27.0

	B3LYP/6311		B3LYP-D3/6311	
	E_{abs}	D_e	E_{abs}	D_e
$\mathbf{w}$	−76.421485		−76.421494	
$\mathbf{e}^{\mathrm{M}}$	−254.235411		−254.239755	
$\mathbf{e}^{\mathrm{M}}\mathbf{w}$	−330.668981	31.7	−330.676090	39.0
$\mathbf{we}^{\mathrm{M}}$	−330.666491	25.2	−330.673871	33.1

1-Dimensional vibrational analysis

For a 1-dimensional vibrational analysis of the OH stretching vibration, we employed point-wise MP2 calculations for monomer structures along the pathway (see main text), deflecting only the O–H bond length by ±0.001 Å from its original value. We thereby obtained the harmonic force constants $f_{\mathrm{OH}}^{\mathrm{loc}}$ as the second derivatives of the electronic energies for a hypothetical, fully localized O–H oscillator. Matching reduced masses $\mu_{\mathrm{OH}}^{\mathrm{loc}}$ were calculated by assuming that the localized vibrations would possess the same wavenumbers ω as their normal-mode ("norm") counterparts:

$$\omega = \frac{1}{2\pi c}\sqrt{\frac{f_{\mathrm{OH}}^{\mathrm{loc}}}{\mu_{\mathrm{OH}}^{\mathrm{loc}}}} = \frac{1}{2\pi c}\sqrt{\frac{f_{\mathrm{OH}}^{\mathrm{norm}}}{\mu_{\mathrm{OH}}^{\mathrm{norm}}}}$$

The resulting values of $\mu_{\mathrm{OH}}^{\mathrm{loc}}$ are largely conformation-independent, supporting the assumption that the OH stretching mode is already of highly localized nature in the normal-mode analysis. The same holds true for the alcoholic OH stretching vibration in the dimers. Hence, the OH stretching motion is well-represented by the local-mode picture in all structures, even when allowing for the cooperative secondary contact.

Table S2 assembles the harmonic O–H stretching wavenumbers and red shifts calculated in the local-mode approach for the different structures along the pathway presented in the main text. By virtue of the nopt structures, the overall dimerization red shifts can be partitioned into two contributing factors: First, the structural deformation of the opt to the nopt monomers found in the dimers; second, the electronic influence of the intermolecular OH$\cdots$O contact. The first step itself again comprises two opposing effects: The torsion of the OH group out of its equilibrium monomer position (see the main text), leading to an increase in stretching wavenumber of about 20 cm^{-1} in the most stable $\mathbf{e}^{\mathrm{M}}$ conformer; and the elongation of the OH bond due to hydrogen bond formation. The increase in wavenumber upon OH torsion is consistent with calculations for $\mathbf{e}^{0}$ which show similar trends.[6] Conversely, OH bond elongation leads to a decrease of the curvature in an anharmonic potential, thus reducing the predicted harmonic frequency at these points. This anharmonic effect strongly overcompensates the torsional one, leading to the overall opt→nopt structural red shift. In $\mathbf{e}^{0}\mathbf{w}$, the torsional displacement is virtually absent (cf. Table 3 of the main text) and the OH bond elongation is much smaller than in the fluorinated cases. Agreement of the 1D analyses with normal-mode calculations carried out at the nopt structures ignoring their non-stationary character is close.

Concerning the dimerization step, if the interaction potential $V^{\mathrm{int}}(r_{\mathrm{OH}})$ between the fluoroethanol and water molecules is linear in r_{OH}, its second derivative vanishes and hence, the

Table S2: Predicted MP2 local-mode vibrational OH stretching frequencies in optimized and non-optimized *gauche* fluoroethanol monomers ($\omega_{\mathbf{e}^z}^{\mathrm{opt}}$ and $\omega_{\mathbf{e}^z}^{\mathrm{nopt}}$, resp.) and dimers ($\omega_{\mathbf{e}^z\mathbf{w}}$) along the pathway presented in the main text. Also given are the structural red shifts between the opt and nopt monomers ($-\Delta\omega^{\mathrm{struc}}$) and the electronic red shifts between the nopt monomers and the dimers ($-\Delta\omega^{\mathrm{nopt}}$). All data from point-wise calculations and in cm^{-1}.

	$\omega_{\mathbf{e}^z}^{\mathrm{opt}}$	$\omega_{\mathbf{e}^z}^{\mathrm{nopt}}$	$-\Delta\omega^{\mathrm{struc}}$	$\omega_{\mathbf{e}^z\mathbf{w}}$	$-\Delta\omega^{\mathrm{nopt}}$
$\mathbf{e}^0\mathbf{w}$	3888	3837	51	3804	33
$\mathbf{e}^{\mathrm{M}}\mathbf{w}$(F)	3880	3800	80	3754	46
$\mathbf{e}^{\mathrm{M}}\mathbf{w}$(H)	3890	3820	70	3792	28
$\mathbf{e}^{\mathrm{M}}\mathbf{w}$(H′)	3887	3821	66	3794	27
$\mathbf{e}^{\mathrm{D}}\mathbf{w}$(H)	3891	3818	73	3789	29
$\mathbf{e}^{\mathrm{D}}\mathbf{w}$(F)	3881	3793	88	3746	47
$\mathbf{e}^{\mathrm{T}}\mathbf{w}$	3881	3780	101	3731	49

Table S3: Predicted MP2 local-mode vibrational OH stretching frequencies in C_s-optimized and non-optimized *trans* fluoroethanol monomers ($\omega_{\mathbf{e}^z}^{\mathrm{opt}}$ and $\omega_{\mathbf{e}^z}^{\mathrm{nopt}}$, resp.) and dimers ($\omega_{\mathbf{e}^z\mathbf{w}}$). Also given are the structural red shifts between the opt and nopt monomers ($-\Delta\omega^{\mathrm{struc}}$) and the electronic red shifts between the nopt monomers and the dimers ($-\Delta\omega^{\mathrm{nopt}}$). All data from point-wise calculations and in cm^{-1}.

	$\omega_{\mathbf{e}^z}^{\mathrm{opt}}$	$\omega_{\mathbf{e}^z}^{\mathrm{nopt}}$	$-\Delta\omega^{\mathrm{struc}}$	$\omega_{\mathbf{e}^z\mathbf{w}}$	$-\Delta\omega^{\mathrm{nopt}}$
$\mathbf{e}^0\mathbf{w}$	3899	3827	71	3807	92
$\mathbf{e}^{\mathrm{M}}\mathbf{w}$	3911	3824	87	3793	118
$\mathbf{e}^{\mathrm{D}}\mathbf{w}$	3911	3827	84	3782	129
$\mathbf{e}^{\mathrm{T}}\mathbf{w}$	3912	3817	95	3756	156

overall second derivative of the dimer potential $V^{\mathrm{dim}} = V^{\mathrm{mon}} + V^{\mathrm{int}}$ is the same as for the monomer. In the harmonic approximation, this affects only the minimum position of the potential, but not the spacing of its energy levels.[7] Thus, any nopt→dimer shift in harmonic vibrational wavenumber upon dimerization must be caused by a non-linearity in $V^{\mathrm{int}}(r_{\mathrm{OH}})$ while any opt→nopt monomer shift must be due to anharmonicity of the OH bond, in addition to other structural relaxation effects such as torsion.

Water OH stretching bands

The spectral assignments of mixed fluoroalcohol/water dimers were made primarily by comparison of the observed and predicted red shifts for the alcoholic OH stretching bands. In principle, it would also be desirable to use the symmetric and asymmetric OH stretching bands of the complexated water molecule to support these assignments. Theoretical predictions of band positions and intensities are directly available from the calculations (see Tab. S4); they show a decreasing red shift of the symmetric water stretch in the $\mathbf{e}^{\mathrm{z}}\mathbf{w}$ structures with increasing fluorination, which likely represents a combined effect of the increasing importance (red-shifting trend) of the primary OH$\cdots$O contact and the decreasing importance (blue-shifting trend) of the secondary OH$\cdots$F contact. Unfortunately, several problems arise in the identification and analysis of these bands:

- **Masking of weak $\mathbf{e}^{\mathrm{z}}\mathbf{w}$ symmetric water bands.** The band centers of the monomeric fluoroethanol-OH and symmetric water stretching vibrations almost coincide (see Tab. 1 of the main text). Due to similar red shifts, the symmetric water stretching bands in the $\mathbf{e}^{\mathrm{z}}\mathbf{w}$ dimers may thus be "masked" by the spectral signatures of the $\mathbf{e}^{\mathrm{z}}\mathbf{e}^{\mathrm{z}}$ acceptors. Furthermore, they are generally predicted to be of relatively low intensity compared to the prominent OH stretching bands of the fluoroethanol donors (cf. Tab. S4) and may be below our detection threshold in $\mathbf{e}^{\mathrm{D}}\mathbf{w}$ and $\mathbf{e}^{\mathrm{T}}\mathbf{w}$. The infrared intensity is predicted to be highest in $\mathbf{e}^{\mathrm{M}}\mathbf{w}$ and considering the predicted red shift of 32 cm^{-1}, it might contribute to the triplet band observed in the experimental spectra (see the main text).

- **Absent $\mathbf{we}^{\mathrm{z}}$ symmetric water bands.** In the water-donor $\mathbf{we}^{\mathrm{z}}$ structures, the symmetric water stretching band is moderately intense and was used for assignment of the respective structure in the $\mathbf{w}/\mathbf{e}^{\mathrm{M}}$ spectra; however, these structures are too unstable to be observed under jet-cooled conditions in the $\mathbf{w}/\mathbf{e}^{\mathrm{D}}$ and $\mathbf{w}/\mathbf{e}^{\mathrm{T}}$ spectra.

- **Masking of asymmetric water bands.** The asymmetric water stretching bands are predicted to be of moderate and almost uniform intensity in all structures and are furthermore spectrally well-separated from the symmetric water and alcoholic OH stretching bands (see Fig. S1). However, the jet spectra show a complicated and extensive signature of rovibrational monomer and homodimer transitions in this region, the exact intensity pattern of which depends on the conditions established in the supersonic expansion. The identification of individual heterodimer bands in this region will thus be difficult. In the

$\mathbf{e}^{\mathrm{M}}$ spectra, one additional feature is visible at 3736 cm^{-1}, red-shifted from the monomer band center by 20 cm^{-1}. Considering the large preference of the $\mathbf{e}^{\mathrm{M}}\mathbf{w}$ over the $\mathbf{we}^{\mathrm{M}}$ structure in the supersonic expansion, we tentatively attribute this band to the former structure. The $\mathbf{e}^{\mathrm{D}}$ and $\mathbf{e}^{\mathrm{T}}$ spectra do, unfortunately, not reveal similar new bands, under the investigated conditions.

- **Harmonic frequency calculations.** The theoretical predictions of the symmetric and asymmetric water stretching bands and their respective hydrogen-bonded counterparts may be principally hampered by the fact that a purely harmonic vibrational model was applied, ignoring any anharmonic coupling between the two vibrational modes.[8] As shown above, the alcoholic OH stretching modes are essentially well-localized one-dimensional oscillators and can thus be expected to suffer less from the neglect of anharmonic couplings with other vibrational modes. Applying the predictions for the water stretching bands to our experimental spectra may thus be somewhat less straightforward when compared to the good agreement in the case of the fluoroethanol bands.

Table S4: MP2/6-311++G(d,p) predictions of OH stretching band red shifts $-\Delta\omega$ (in cm^{-1}) and infrared intensities I (in km/mol) of fluoroethanol ($\mathbf{e}^{\mathrm{z}}$) and water ($\mathbf{w}$) in mixed dimers relative to the corresponding monomer vibrations. Indices "s" and "a" indicate that the water vibration correlates with the symmetric ("$\mathbf{w}$(s)") and asymmetric ("$\mathbf{w}$(a)") stretching vibration of the water monomer, respectively. Observed transitions are printed in boldface.

	$-\Delta\omega_{\mathbf{e}^{\mathrm{z}}}$	I	$-\Delta\omega^{\mathrm{s}}_{\mathbf{w}}$	I	$-\Delta\omega^{\mathrm{a}}_{\mathbf{w}}$	I
$\mathbf{e}^{\mathrm{M}}\mathbf{w}$	126	**378**	32	61	26	**124**
$\mathbf{we}^{\mathrm{M}}$	9	55	122	**230**	36	100
$\mathbf{e}^{\mathrm{D}}\mathbf{w}$	135	**435**	19	21	19	111
$\mathbf{we}^{\mathrm{D}}$	6	58	92	147	33	108
$\mathbf{e}^{\mathrm{T}}\mathbf{w}$	150	**491**	17	14	20	103
$\mathbf{we}^{\mathrm{T}}$	9	58	52	86	28	106

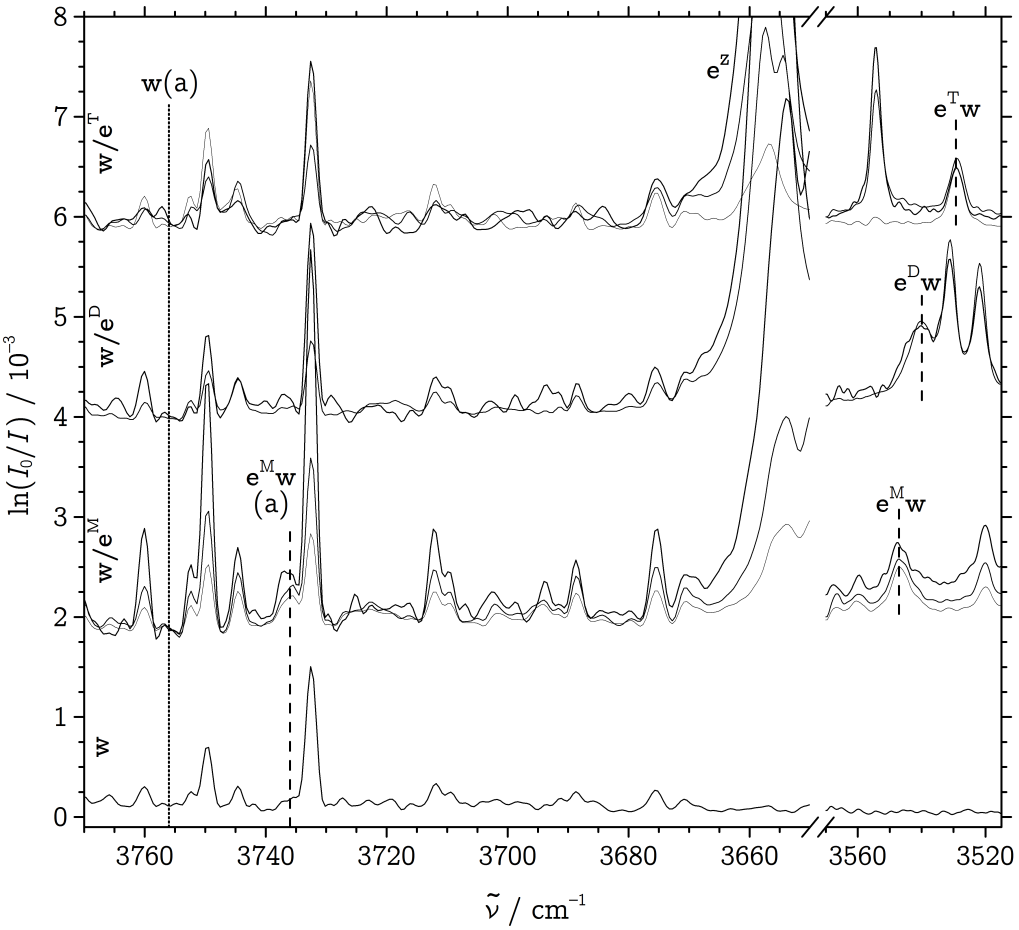

Figure S1: Spectral region of the asymmetric water stretching vibration, assembling all spectra from Figs. 1–3 of the main text, scaled to equal intensities of the respective $\mathbf{e}^{\mathrm{z}}\mathbf{w}$ bands. "$\mathbf{e}^{\mathrm{z}}$" marks the fluoroethanol monomer bands, "$\mathbf{w}$(a)" the band center of the asymmetric stretching vibration of monomeric water at 3756 cm^{-1}. "$\mathbf{e}^{\mathrm{M}}\mathbf{w}$(a)" indicates our rather tentative assignment of the asymmetric water stretching band in the $\mathbf{e}^{\mathrm{M}}\mathbf{w}$ structure (see text).

References

[1] Frank Jensen. Estimating the Hartree-Fock limit from finite basis set calculations. *Theor. Chem. Acc.*, 113:267–273, 2005.

[2] Amir Karton and Jan Martin. Comment on: "Estimating the Hartree-Fock limit from finite basis set calculations" [Jensen F (2005) Theor Chem Acc 113:267]. *Theor. Chem. Acc.*, 115:330–333, 2006.

[3] Iain D. Mackie and Gino A. DiLabio. Approximations to complete basis set-extrapolated, highly correlated non-covalent interaction energies. *J. Chem. Phys.*, 135(13):134318, 2011.

[4] Wim Klopper, Frederick R. Manby, Seiichiro Ten-No, and Edward F. Valeev. R12 methods in explicitly correlated molecular electronic structure theory. *Int. Rev. Phys. Chem.*, 25(3):427–468, 2006.

[5] Oliver Marchetti and Hans-Joachim Werner. Accurate calculations of intermolecular interaction energies using explicitly correlated wave functions. *Phys. Chem. Chem. Phys.*, 10:3400–3409, 2008.

[6] Tobias N. Wassermann and Martin A. Suhm. Ethanol Monomers and Dimers Revisited: A Raman Study of Conformational Preferences and Argon Nanocoating Effects. *J. Phys. Chem. A*, 114(32):8223–8233, 2010.

[7] Shi Yi Liu and Clifford E. Dykstra. A theory of vibrational transition frequency shifts due to hydrogen bonding. *J. Phys. Chem.*, 90(14):3097–3103, 1986.

[8] G. Avila, J.M. Fernández, B. Maté, G. Tejeda, and S. Montero. Ro-vibrational Raman Cross Sections of Water Vapor in the OH Stretching Region. 196(1):77–92, 1999.